J. Fluid Mech. (1991), *vol.* 226, *pp.* 125–148
Printed in Great Britain

Viscous flow in a channel with periodic cross-bridging fibres: exact solutions and Brinkman approximation

By RUEY-YUG TSAY[1] AND SHELDON WEINBAUM[2]

[1] Department of Chemical Engineering, The City College of the City University of New York, New York, NY 10031, USA

[2] Department of Mechanical Engineering, The City College of the City University of New York, New York, NY 10031, USA

(Received 20 March 1990 and in revised form 4 October 1990)

A general solution of the three-dimensional Stokes equations is developed for the viscous flow past a square array of circular cylindrical fibres confined between two parallel walls. This doubly periodic solution, which is an extension of the theory developed by Lee & Fung (1969) for flow around a single fibre, successfully describes the transition in behaviour from the Hele-Shaw potential flow limit (aspect ratio $B \ll 1$) to the viscous two-dimensional limiting case ($B \gg 1$, Sangani & Acrivos 1982) for the hydrodynamic interaction between the fibres. These results are also compared with the solution of the Brinkman equation for the flow through a porous medium in a channel. This comparison shows that the Brinkman approximation is very good when $B > 5$, but breaks down when $B \leqslant O(1)$. A new interpolation formula is proposed for this last regime. Numerical results for the detailed velocity profiles, the drag coefficient f, and the Darcy permeability K_p are presented. It is shown that the velocity component perpendicular to the parallel walls is only significant within the viscous layers surrounding the fibres, whose thickness is of the order of half the channel height B'. One finds that when the aspect ratio $B > 5$, the neglect of the vertical velocity component v_z can lead to large errors in the satisfaction of the no-slip boundary conditions on the surfaces of the fibres and large deviations from the approximate solution in Lee (1969), in which v_z and the normal pressure field are neglected. The numerical results show that the drag coefficient of the fibrous bed increases dramatically when the open gap between adjacent fibres Δ' becomes smaller than B'. The predictions of the new theory are used to examine the possibility that a cross-bridging slender fibre matrix can exist in the intercellular cleft of capillary endothelium as proposed by Curry & Michel (1980).

1. Introduction

The problem of viscous flow in a closely spaced parallel-walled channel with cylindrical obstacles has attracted considerable attention since Hele-Shaw in 1898 first observed that the streamlines for this flow accurately reproduced the lines of force around a metal cylinder in a dielectric medium in a magnetic field. This behaviour was then explained by Stokes who mathematically showed that if the spacing between the walls $2B'$ was small compared to the diameter $2a$ of the cylinder, the vertical component of the velocity could be neglected and the governing equation for the viscous flow in planes parallel to the boundaries was a potential flow equation. This equation could be satisfied everywhere except in a thin boundary-layer region

near the cylinder surface where the no-slip conditions could not be satisfied. Using perturbation theory and matched asymptotic expansions Thompson (1968) was able to show for $B = B'/a \ll 1$ there was a small layer near the cylinder of thickness $O(B')$ where the vertical velocity did not vanish and the neglected viscous terms were required to satisfy the boundary conditions. A major advance in the analysis of this problem was then developed by Lee & Fung (1969) who wished to treat the more complicated problem where the aspect ratio of the cylinders B was of $O(1)$. The motivation for this study was the flow of blood around the septal posts in pulmonary alveoli where the aspect ratio of the posts was typically 2. An accurate infinite series solution to the three-dimensional Stokes equation for the flow past a single circular cylinder was developed and numerical results based on a truncated series were calculated for aspect ratios $B \leqslant 5$. An approximate two-term solution was also presented which neglected the vertical velocity component and approximately satisfied the no-slip conditions on the cylinder provided $B \leqslant 1$. However, for $B = 5$ the error in the no-slip condition on the cylinder surface at the midplane for the two-term approximation was nearly 50%. This two-term approximation was then applied by Lee (1969) for a two-dimensional periodic array of circular cylinders as a model for the septal posts in alveolar sheet flow. The two-term approximate theory in Lee (1969) also broke down if the spacing between the cylinder surfaces Δ' was comparable with or smaller than the channel height $2B'$.

In the present study a more general analysis of the channel flow problem for the doubly periodic array of cylinders is undertaken which expands the solution approach developed in Lee & Fung (1969) and Lee (1969). In particular, we are interested in the flow in a parallel-walled channel in which the aspect ratio of the cylinders covers the entire range from $B \leqslant 1$ to $B \gg 1$ and solidity ratios where $\Delta/2B \leqslant O(1)$. In the limit where $\Delta/2B \ll 1$ this theory should approach the large body of solutions for the two-dimensional viscous flow past a doubly periodic array of infinite cylinders (Kuwabara 1959; Happel 1959; Spielman & Goren 1968; Sangani & Acrivos 1982; Drummond & Tahir 1984). The principal simplification in Lee & Fung (1969) for the flow past a single cylinder is that the outer potential flow is a uniform Poiseuille flow at infinity. In this limit the upstream flow for the velocity potential in planes parallel to the boundaries has a simple $\sin\theta$ dependence in cylindrical coordinates. For an array of cylinders, an infinite series of higher-order harmonic functions in θ are required and solutions which accurately satisfy the no-slip conditions for all three velocity components on the surface of the cylinders are sought. We believe that the new solutions developed herein are of fundamental interest to fluid mechanicians because they describe the transition in behaviour from the irrotational Hele-Shaw potential flow limit to the two-dimensional limiting behaviour for $B \gg 1$ described above. This change in behaviour, which is related to the thickness of the viscous layers wherein the flow adjusts to satisfy the no-slip conditions on the surfaces of the fibres, arises strictly from the geometric lengthscales in the problem, and should not be confused with the more common viscous–inviscid interaction associated with traditional boundary layers that scale with the Reynolds number.

Low-Reynolds-number flows in pores or channels filled with a porous matrix of fibrous material have frequently been approximated using a Brinkman equation (Brinkman 1947; Bird, Stewart & Lightfoot 1960; Neale & Nader 1974). A summary of these applications is given in Ethier & Kamm (1989), who have used this Brinkman approach to model flow through gel-filled channels. In the Brinkman equation the effect of the fibre matrix is represented by a distributed body force

based on Darcy's law for an infinite medium. It is well recognized that the applicability of the equation requires that the microscopic internal lengthscale of the medium (spacing between fibres) be small compared to the characteristic distance over which the macroscopic average velocity and pressure varies. Larson & Higdon (1986) using detailed numerical calculations have shown that the Brinkman approach is a good approximation for shear flow over an isotropic fibre matrix. There is to our knowledge no previous model for examining the validity and limitations of the Brinkman equation for approximating bounded porous-media flows. In particular, one wishes to study the behaviour of the Brinkman equation as the fibre spacing is varied relative to the characteristic macroscopic length, the channel height. We shall show that in the dilute fibre limit the two-term approximation used in Lee (1969) provides a more accurate description of the drag due to the fibres and channel walls than the Brinkman equation. It is thus possible to develop a new highly accurate interpolation formula for the effective viscosity of the channel using a curve fit which asymptotically approaches the analytic limiting expressions of Lee and Sangani & Acrivos. This formula is superior to Brinkman's approximation for a periodic fibre array in which $B \leqslant O(1)$.

The motivation for the present study derives from a recent paper by Tsay, Weinbaum & Pfeffer (1989) in which a new three-dimensional model has been proposed for capillary filtration through the clefts between endothelial cells in continuous capillaries. These clefts are believed to be the principal pathway for the transcapillary movement of water and small solutes (Curry 1984, 1986; Michel 1985). The intercellular clefts between adjacent membranes of vascular endothelial cells are narrow channels of typically 20–25 nm gap height and depth (length along channel midplane) which can vary from 400 nm for capillaries to 2000 nm for arterial endothelium. Except for localized constrictions associated with intramembranous junction protein arrays, the gap height between membranes is of remarkable uniformity. A molecular-level theory which attempts to relate the intramembranous protein structure to the spacing of the membranes is developed in Weinbaum (1980). The inability of a simple parallel or constricted channel geometry to explain the measured water and solute permeability data of capillaries in various tissues has led Curry & Michel (1980) to propose that the uniform portion of the cleft is filled with a proteoglycan matrix of cross-bridging fibres of approximately 0.6 nm radius. Rough estimates of the filtration resistance of this fibre matrix in Tsay *et al.* (1989) based on the two-term asymptotic solution in Lee (1969) have suggested that the Carman–Kozeny equation that had previously been used to describe the flow through the cross-bridging matrix may be totally inappropriate since it describes an infinite matrix and neglects the hydrodynamic interaction between the fibres and the channel walls, which is the dominant effect in the dilute fibre limit. Michel (1985) and Curry (1986) have also suggested that the fibres, as opposed to the junctional constrictions, serve as the primary molecular sieve for larger solute molecules. The aspect ratio B of these fibres based on the dimensions cited is 18.3 ($B' = 22$ nm, $a = 0.6$ nm). Estimates of the typical spacing Δ' between fibres for them to serve as the molecular filter lie in the range of 6 to 10 nm. Thus the values of both B and Δ/B lic considerably outside the range of validity of the approximate theory in Lee (1969) for a cross-bridging periodic fibre array. The periodic fibre structure is also of interest in another context. Silberberg (1987) and Firth, Bauman & Sibley (1983) have proposed, based on electron microscopic studies, that the uniformity of spacing may be due to a small volume fraction of cross-bridging proteins that span the channel. The aspect ratio B of these larger cross-bridging molecules is 2–3 and thus similar to

the septal posts in lung alveoli. Results will be presented herein to examine the feasibility of both these cross-bridging molecular networks.

This paper is presented in five sections. The general formulation of the problem is presented in §2. Section 3 describes the procedure for obtaining accurate solutions for the flow through a doubly periodic fibre array. The solution for the effective viscosity is also given. The principal results are presented in §4 where the present results are compared with various approximate solutions. Finally §5 discusses the implications of these results for the biological problem that motivated this study.

2. Formulation

For flow through a fibre matrix confined between two parallel plates, Fung & Sobin (1969) have defined the following 'macroscopic' relationship between the pressure gradient and the fluid velocity:

$$\overline{\nabla' P'} = -(3\mu_{\text{eff}}/B'^2)\,\bar{U}, \tag{1}$$

where the prime indicates dimensional coordinates, and the overbar denotes an average value over a region which is small compared with the macroscopic lengthscale, yet is large enough to level off the microscopic heterogeneity. For a periodic fibre arrangement, the average is taken over one periodic unit. The effective viscosity μ_{eff} equals μf, where f represents the influence of the fibres. In general f is a function of the configuration of the fibre array, the fibre volume fraction S and the aspect ratio B. To determine f one must first obtain a solution for the local flow field in the periodic unit. The contribution to f arises from two sources, the resistance of the fibres and the increased resistance of the wall due to the velocity disturbance generated by the fibre–wall interaction.

It is convenient to formulate the problem in terms of dimensionless coordinates. In the following, all the lengths are scaled relative to the fibre radius a. The fluid velocity V is made dimensionless with respect to the superficial velocity $\bar{U}$ and the fluid pressure P with respect to a characteristic viscous stress $\mu\bar{U}/a$. A idealized configuration of the intercellular cross-bridging fibre array is shown in figure 1. This structure is similar to the internal geometry of the pulmonary alveolar septa proposed by Lee (1969). Let (x, y, z) be a set of Cartesian coordinates and (r, θ, z) be a set of cylindrical coordinates. These two sets of coordinates have the same origin. Let (α, β) designate a particular fibre in the periodic array. The centre of the $\alpha\beta$th fibre is located at $Z_{\alpha\beta}$, where Z is a complex plane with

$$Z = x + \mathrm{i}y = r\,\mathrm{e}^{\mathrm{i}\theta} \quad \text{and} \quad Z_{\alpha\beta} = 2\alpha\bar{\omega}_1 + 2\beta\bar{\omega}_2 = R_{\alpha\beta}\exp(\mathrm{i}\psi_{\alpha\beta}).$$

Here $$2\bar{\omega}_1 = \omega_1 - \mathrm{i}\omega_2, \quad \bar{\omega}_2 = \omega_1 + \mathrm{i}\omega_2 \quad \text{and} \quad \omega_1 = \omega_2 = \tfrac{1}{2}W$$

for a square array. $(r_{\alpha\beta}, \theta_{\alpha\beta}, z)$ are the local coordinates corresponding to the $\alpha\beta$th fibre.

For an incompressible creeping flow, the non-dimensionalized continuity equation and Stokes equation are

$$\nabla \cdot V = 0, \tag{2}$$

$$\nabla^2 V = \nabla P. \tag{3}$$

The fluid velocity V must satisfy the no-slip conditions on the surfaces of the fibres and the channel walls:

$$V = 0 \quad \text{at} \quad r_{\alpha\beta} = 1, \tag{4}$$

$$V = 0 \quad \text{at} \quad z = \pm B, \tag{5}$$

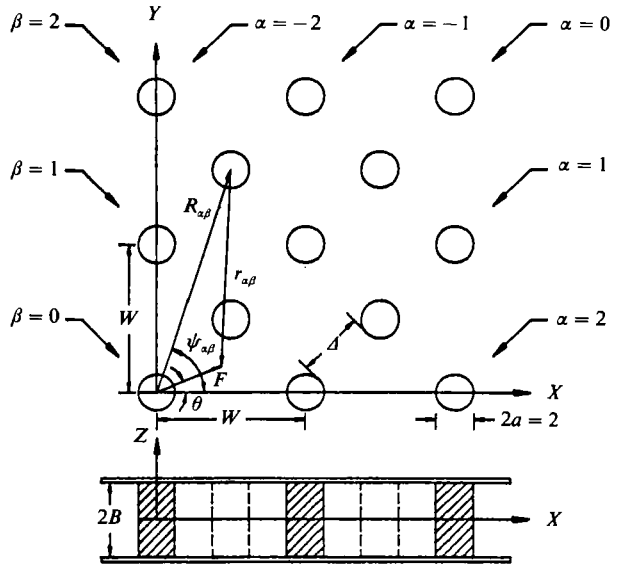

FIGURE 1. A top view and a side view of the idealized periodic configuration for the cross-bridging fibre array in an intercellular channel. All the lengths are scaled relative to the fibre radius a.

and the total flux Q is given by

$$\frac{Q}{2B'W'\bar{U}} = 1 = \frac{1}{2BW}\int_{-B}^{+B}\int_{1}^{W-1} v_\theta(\theta = \tfrac{1}{2}\pi)\,\mathrm{d}r\,\mathrm{d}z. \tag{6}$$

Using (2) and (3), one can show that P is a harmonic function and the components of V are biharmonic functions.

3. Method of solution

3.1. *General solution for Stokes flow confined between two flat plates*

A general solution of (2) and (3) in cylindrical coordinates which satisfies the no-slip conditions on the two channel walls is given by Lee & Fung (1969) as

$$P = -\frac{2}{B}\left\{\frac{\phi_0}{B} + \mathrm{Re}\left[\sum_{n=1}^{\infty}\phi_n\frac{\cos\alpha_n z}{\cos\alpha_n B}\right]\right\}, \tag{7}$$

$$v_r = -\left(\frac{1}{r}\frac{\partial\psi_0}{\partial\theta}\right)\left(1-\frac{z^2}{B^2}\right) - \mathrm{Re}\left[\sum_{n=1}^{\infty}\frac{1}{\alpha_n^2}\left(\frac{\partial\phi_n}{\partial r}\right)\left(\frac{\mathrm{d}q_n}{\mathrm{d}z}\right)\right] - \sum_{n=0}^{\infty}\left(\frac{1}{r}\frac{\partial\bar{\psi}_n}{\partial\theta}\right)\cos\lambda_n z, \tag{8}$$

$$v_\theta = -\left(\frac{\partial\psi_0}{\partial r}\right)\left(1-\frac{z^2}{B^2}\right) - \mathrm{Re}\left[\sum_{n=1}^{\infty}\frac{1}{\alpha_n^2}\left(\frac{1}{r}\frac{\partial\phi_n}{\partial\theta}\right)\left(\frac{\mathrm{d}q_n}{\mathrm{d}z}\right)\right] + \sum_{n=0}^{\infty}\left(\frac{\partial\bar{\psi}_n}{\partial r}\right)\cos\lambda_n z, \tag{9}$$

$$v_z = \mathrm{Re}\left[\sum_{n=1}^{\infty}\phi_n q_n\right], \tag{10}$$

where

$$q_n(z) = \left(\frac{\sin\alpha_n z}{\sin\alpha_n B}\right) - \left(\frac{z\cos\alpha_n z}{B\cos\alpha_n B}\right). \tag{11}$$

α_n and λ_n are eigenvalues which satisfy the following equations:

$$\sin 2\alpha_n B = 2\alpha_n B, \tag{12}$$

$$\lambda_n = (2n+1)\frac{\pi}{2B}, \quad n = 0, 1, 2, \ldots. \tag{13}$$

Here all the eigenvalues α_n are complex except $\alpha_0 = 0$. Approximate values for α_n are given by the equation

$$2\alpha_n B = (2n+\tfrac{1}{2})\pi \pm i \ln[(4n+1)\pi], \quad n = 1, 2, 3, \ldots.$$

The eigenfunctions ϕ_0, ψ_0, ϕ_n, and $\bar{\psi}_n$ satisfy the following differential equations:

$$E^2\psi_0 = 0, \quad E^2\phi_0 = 0, \tag{14}$$

$$E^2\phi_n - \alpha_n^2\phi_n = 0, \quad n = 1, 2, \ldots, \tag{15}$$

$$E^2\bar{\psi}_n - \lambda_n^2\bar{\psi}_n = 0, \quad n = 0, 1, 2, \ldots, \tag{16}$$

where

$$E^2 = \frac{\partial^2}{\partial r^2} + \frac{1}{r}\frac{\partial}{\partial r} + \frac{1}{r^2}\frac{\partial^2}{\partial \theta^2}.$$

The fundamental solutions given by (7)–(10) are a superposition of three contributions: the terms containing ϕ_0 and ψ_0 are the zero-eigenvalue biharmonic solutions for $\alpha_0 = 0$, which correspond to the irrotational Hele-Shaw flow; the terms containing ϕ_n with $n \geqslant 1$ are biharmonic solutions, which describe the vertical component of the velocity in the z-direction induced by the motion of the vorticity layer past the fibres inside the channel; the terms containing $\bar{\psi}_n$ are the rotational harmonic solutions, which are required to satisfy the no-slip boundary condition on the surface of each fibre. The $\bar{\psi}_n$ harmonic solutions do not contribute to the pressure field, whereas the ϕ_n solutions do not contribute to the z-component of the vorticity.

The solution of (14)–(16) can be obtained by separation of variables. These separable solutions are

$$\left.\begin{aligned}
&\phi_0, \psi_0: \quad r^{-m}\cos m\theta, \quad r^{-m}\sin m\theta, \quad r^m\cos m\theta, \quad r^m\sin m\theta, \\
&\phi_n: \quad K_m(\alpha_n r)\cos m\theta, \quad K_m(\alpha_n r)\sin m\theta, \quad I_m(\alpha_n r)\cos m\theta, \quad I_m(\alpha_n r)\sin m\theta, \\
&\bar{\psi}_n: \quad K_m(\lambda_n r)\cos m\theta, \quad K_m(\lambda_n r)\sin m\theta, \quad I_m(\lambda_n r)\cos m\theta, \quad I_m(\lambda_n r)\sin m\theta,
\end{aligned}\right\} \tag{17}$$

where I_m and K_m are modified Bessel functions of the first and second kind of order m. The functions ϕ_0, ψ_0, ϕ_n, and $\bar{\psi}_n$ are linear combinations of these separable solutions. For flow around a single fibre, Lee & Fung (1969) showed that the $m = 1$ terms are sufficient to provide a complete solution. However, for flow through a fibre array, the problem is considerably more complicated since an infinite series of terms with $m > 1$ are required in the solutions for ϕ_0, ψ_0, ϕ_n and $\bar{\psi}_n$ to describe the interaction between the fibres.

3.2. *Stokes flow past a square array of cylindrical fibres inside a channel*

Some of the separable solutions in (17) can be eliminated by applying the boundary conditions at $r \to \infty$. Since the flow field is bounded everywhere, the terms including r^m $(m > 1)$, $I_m(\alpha_n r)$, and $I_m(\lambda_n r)$ for $(m \geqslant 0)$ must be excluded. The fundamental solutions for ϕ_n and $\bar{\psi}_n$ thus reduce to the more limited set

$$\phi_n: \quad K_m(\alpha_n r_{\alpha\beta})\cos m\theta_{\alpha\beta}, \quad K_m(\alpha_n r_{\alpha\beta})\sin m\theta_{\alpha\beta}, \tag{18}$$

$$\bar{\psi}_n: \quad K_m(\lambda_n r_{\alpha\beta})\cos m\theta_{\alpha\beta}, \quad K_m(\lambda_n r_{\alpha\beta})\sin m\theta_{\alpha\beta}. \tag{19}$$

The doubly periodic functions for ϕ_n and $\bar{\psi}_n$ can be obtained by summing the functions in (18) and (19) over all possible α, β. Similarly, one could construct the quasi-doubly periodic functions for ϕ_0 and ψ_0 by summing terms involving r^{-m} $(m \geqslant -1)$ over α, β. However, since ϕ_0 and ψ_0 are harmonic functions

corresponding to the irrotational Hele-Shaw flow, a simpler alternative is to take advantage of the periodicity properties of the Weierstrass zeta function $\zeta(Z)$ as proposed earlier in Lee (1969).

According to the Cauchy–Reimann theorem, one knows that there is a function Φ of the complex variable Z which satisfies

$$\Phi(Z) = \phi_0 + \mathrm{i}\psi_0. \tag{20}$$

The function $\Phi(Z)$, which is an integral of an elliptic function for a doubly periodic fibre array, can be expressed as a linear combination of the Weierstrass zeta function $\zeta(Z)$ and its derivatives (Whittaker & Watson 1944; Lee 1969):

$$\Phi(Z) = b_0 Z + \sum_{m=1}^{\infty} b_n \zeta^{(m)}(Z), \tag{21}$$

where

$$\zeta(Z) = \frac{1}{Z} + \sum_{\alpha,\beta}{}' \left\{ \frac{1}{(Z - Z_{\alpha\beta})} + \frac{1}{Z_{\alpha\beta}} + \frac{Z}{Z_{\alpha\beta}^2} \right\}, \tag{22}$$

$$\zeta(Z)^{(m)} = \frac{(-1)^m}{m!} \left(\frac{\mathrm{d}^m \zeta}{\mathrm{d}Z^m} \right). \tag{23}$$

The symbol $\sum'_{\alpha,\beta}$ is used to denote the summation over all α, β with the exception of the origin $\alpha = \beta = 0$. The function $\zeta(Z)$ is a quasi-periodic function:

$$\zeta(Z + 2\alpha\bar{\omega}_1 + 2\beta\bar{\omega}_2) = \zeta(Z) + 2\alpha\eta_1 + 2\beta\eta_2. \tag{24}$$

The derivatives of $\zeta(Z)$ are doubly periodic functions with periods $2\bar{\omega}_1$ and $2\bar{\omega}_2$, where and $\eta_1 \bar{\omega}_2 - \eta_2 \bar{\omega}_1 = \frac{1}{2}\pi\mathrm{i}$. Using symmetry conditions at the x- and y-axes, terms involving $\zeta^{(2m-1)}$, $K_{2m}(\alpha_n r_{\alpha\beta}) \cos 2m\theta_{\alpha\beta}$, $K_m(\alpha_n r_{\alpha\beta}) \sin m\theta_{\alpha\beta}$, $K_m(\lambda_n r_{\alpha\beta}) \cos m\theta_{\alpha\beta}$, $K_{2m}(\lambda_n r_{\alpha\beta}) \sin 2m\theta_{\alpha\beta}$ in (18), (19), and (21) must vanish. This leads to the following expressions for $\Phi(Z)$, ϕ_n and $\bar{\psi}_n$:

$$\left.\begin{aligned} \Phi(Z) &= b_0 Z + \sum_{m=1}^{\infty} b_n \zeta^{(2m-2)}(Z), \\ \phi_n &= \sum_{m=1}^{\infty} d_{nm} [K_{2m-1}(\alpha_n r) \cos(2m-1)\theta + \sum_{\alpha,\beta}{}' K_{2m-1}(\alpha_n r_{\alpha\beta}) \cos(2m-1)\theta_{\alpha\beta}], \\ \bar{\psi}_n &= \sum_{m=1}^{\infty} c_{nm} [K_{2m-1}(\lambda_n r) \sin(2m-1)\theta + \sum_{\alpha,\beta}{}' K_{2m-1}(\lambda_n r_{\alpha\beta}) \sin(2m-1)\theta_{\alpha\beta}]. \end{aligned}\right\} \tag{25}$$

Substituting (25) into (7)–(10), one has a general solution for a doubly periodic flow field.

In order to apply the no-slip conditions on the surface of the fibres we need to transform the $(r_{\alpha\beta}, \theta_{\alpha\beta}, z)$ coordinates in (25) into a common coordinate system (r, θ, z). The Weierstrass zeta function and its derivatives are transformed according to the binomial theorem

$$\frac{1}{(Z - Z_{\alpha\beta})^m} = \sum_{p=0}^{\infty} \frac{(m+p-1)!}{p!(m-1)!} \frac{(-1)^m Z^p}{Z_{\alpha\beta}^{(m+p)}}. \tag{26}$$

The transformation of the modified Bessel functions can be performed using Graf's generalization of Neumann's addition theorem (Watson 1980):

$$K_m(\alpha r_{\alpha\beta}) \begin{matrix} \sin(m\theta_{\alpha\beta}) \\ \cos(m\theta_{\alpha\beta}) \end{matrix} = \sum_{p=-\infty}^{\infty} K_{m+p}(\alpha R_{\alpha\beta}) I_p(\alpha r) \begin{matrix} \sin(p\theta - (m+p)\psi_{\alpha\beta}) \\ \cos(p\theta - (m+p)\psi_{\alpha\beta}) \end{matrix}. \tag{27}$$

Both of these transformations converge when $|Z| < |Z_{\alpha\beta}|$. After the transformation, (25) becomes

$$\left.\begin{aligned}
\psi_0 &= -b_0\left[r\sin\theta + \sum_{m=1}^{\infty}\frac{\sin(2m-1)\theta}{2m-1}\left(b_m r^{-(2m-1)} + \sum_{p=1}^{\infty} A_{mp} b_p r^{(2m-1)}\right)\right] \\
\bar{\psi}_n &= -\frac{b_0}{\lambda_n}\sum_{m=1}^{\infty}\sin(2m-1)\theta\left[c_{nm}\frac{K_{2m-1}(\lambda_n r)}{K_{2m-1}(\lambda_n)} + \sum_{p=1}^{\infty} B_{nmp} c_{np}\frac{I_{2m-1}(\lambda_n r)}{I_{2m-1}(\lambda_n)}\right], \\
\phi_n &= -\frac{b_0}{\alpha_n}\sum_{m=1}^{\infty}\cos(2m-1)\theta\left[d_{nm}\frac{K_{2m-1}(\alpha_n r)}{K_{2m-1}(\alpha_n)} - \sum_{p=1}^{\infty} D_{nmp} d_{np}\frac{I_{2m-1}(\alpha_n r)}{I_{2m-1}(\alpha_n)}\right]
\end{aligned}\right\} \quad (28)$$

where

$$A_{11} = 0,$$

$$A_{mp} = \frac{(2m+2p-3)!}{(2m-2)!\,(2p-1)!}\sum_{\alpha,\beta}'' G_{\alpha\beta}\frac{\cos(2m+2p-2)\psi_{\alpha\beta}}{R_{\alpha\beta}^{(2m+2p-2)}},$$

$$B_{nmp} = \frac{I_{2m-1}(\lambda_n)}{K_{2p-1}(\lambda_n)}\sum_{\alpha,\beta}'' G_{\alpha\beta}[K_{2m+2p-2}(\lambda_n R_{\alpha\beta})\cos(2m+2p-2)\psi_{\alpha\beta} - K_{2m-2p}(\lambda_n R_{\alpha\beta})\cos(2m-2p)\psi_{\alpha\beta}],$$

$$D_{nmp} = \frac{I_{2m-1}(\alpha_n)}{K_{2p-1}(\alpha_n)}\sum_{\alpha,\beta}'' G_{\alpha\beta}[K_{2m+2p-2}(\alpha_n R_{\alpha\beta})\cos(2\mathrm{m}+2\mathrm{p}-2)\psi_{\alpha\beta} + K_{2m-2p}(\alpha_n R_{\alpha\beta})\cos(2m-2p)\psi_{\alpha\beta}],$$

and

$$G_{\alpha\beta} = 4 \text{ for fibres not located on the } x\text{- or } y\text{-axis}$$
$$= 2 \text{ for fibres located on the } x\text{- or } y\text{-axis.}$$

The notation $\sum_{\alpha,\beta}''$ denotes a summation over all possible fibre positions in the first quadrant, except the one at the origin. Notice that according to the formula for A_{mp},

$$A_{11} = \sum_{\alpha,\beta}''\frac{\cos\psi_{\alpha\beta}}{R_{\alpha\beta}^2} = \frac{S}{\pi}\mathrm{Re}\,[e^{i\pi/2}S_2],$$

where S_2 is the non-absolutely-convergent term evaluated by Rayleigh (1892) and Perrins, McKenzie & McPhedran (1979). Since the terms involving A_{11} cancel out when ϕ_0 is transformed from (25) into (28), we have set $A_{11} = 0$. Rayleigh's convergence difficulties arose from an incorrect assessment of the macroscopic boundary integral, which has been discussed in O'Brien (1979).

By substituting (28) back into (7)–(10) and apply boundary conditions (4) and (6), one should be able to obtain the unknown coefficients in (28). However, because the set of solutions in (7)–(10) involves three different sets of independent functions of z, the no-slip condition on the fibre surface cannot be applied in a straightforward manner. One could attempt to satisfy the no-slip conditions using numerical boundary collocation methods as described in Weinbaum, Ganatos & Yan (1990). However, since this problem is three-dimensional, this would require many grid points and there is no guarantee of convergence. One alternative way which does guarantee convergence is to expand the z-dependence in each velocity component in terms of a complete set of orthogonal functions. For the v_r and v_θ velocity components, the $\cos\lambda_n z$ form a complete set of orthogonal functions. For the v_z velocity component, we follow the procedure of Lee & Fung (1969) for the single fibre case and introduce the function Y_n,

$$Y_n(z) = \frac{1}{\sqrt{2}}\left[\frac{\sin\nu_n z}{\sin\nu_n B} - \frac{\sinh\nu_n z}{\sinh\nu_n B}\right], \quad (29)$$

where ν_n are the positive eigenvalues obtained from the following equation:

$$\tan \nu_n B = \tanh \nu_n B. \tag{30}$$

Approximate values of ν_n are given by $(n+\frac{1}{4})(\pi/B)$, $n = 1, 2, 3, \ldots$. The function Y_n has the proper orthogonality properties because $Y_n(\pm B) = \mathrm{d}Y_n(\pm B)/\mathrm{d}z = 0$ and it is an odd function. The various functions of z appearing in (7)–(10) can now be expressed as infinite series in $\cos \lambda_n z$ or $Y_n(z)$, see Appendix.

Using the foregoing results, one can express each velocity component in (8)–(10) in the form of a doubly infinite series:

$$\left.\begin{aligned} u &= \sum_{n=0}^{\infty} \sum_{m=1}^{\infty} \bar{U}_{mn}(r) \cos(2m-1)\theta \cos \lambda_n z, \\ v &= \sum_{n=0}^{\infty} \sum_{m=1}^{\infty} \bar{V}_{mn}(r) \sin(2m-1)\theta \cos \lambda_n z, \\ w &= \mathrm{Re}\left[\sum_{n=1}^{\infty} \sum_{m=1}^{\infty} \bar{W}_{mn}(r) \cos(2m-1)\theta Y_n\right]. \end{aligned}\right\} \tag{31}$$

The expressions for $\bar{U}_{mn}$, $\bar{V}_{mn}$ and $\bar{W}_{mn}$ are given in the Appendix.

3.3. *Numerical solution for unknown coefficients*

In order to solve for the unknown coefficients in the expressions for $\bar{U}_{mn}$, $\bar{V}_{mn}$ and $\bar{W}_{mn}$ in (31), we first truncate the doubly infinite series at $n = N$ and $m = M$. The truncated series is then required to satisfy the no-slip conditions on the surface of the fibre at the origin. Owing to the periodicity, this automatically satisfies the no-slip condition on all the other fibres. By applying the orthogonality of the functions Y_n, $\sin m\theta$, and $\cos m\theta$, we obtain

$$\left.\begin{aligned} &\sum_{p=1}^{M} (A_{mp} + \delta_{mp}) b_p + \frac{(2m-1)}{\lambda_n l_n} \sum_{p=1}^{M} (B_{nmp} + \delta_{mp}) c_{np} \\ &\quad - \mathrm{Re}\left[\sum_{j=1}^{N} \frac{e_{jn}}{\alpha_j^2 l_n} \sum_{p=1}^{M} (DK\alpha_{jp}\delta_{mp} - DI\alpha_{jm} D_{jmp}) d_{jp} = -\delta_{m1}\right] \\ &\qquad\qquad (m = 1, M,\ n = 0, N), \\ &\sum_{p=1}^{M} (A_{mp} - \delta_{mp}) b_p + \frac{1}{\lambda_n l_n} \sum_{p=1}^{M} (DK\lambda_{np}\delta_{mp} + DI\lambda_{nm} B_{nmp}) c_{np} \\ &\quad - \mathrm{Re}\left[\frac{(2m-1)}{l_n} \sum_{j=1}^{N} \frac{e_{jn}}{\alpha_j^2} \sum_{p=1}^{M} (\delta_{mp} - D_{jmp}) d_{jp} = -\delta_{m1}\right] \quad (m = 1, M,\ n = 0, N) \\ &\mathrm{Re}\left[\sum_{j=1}^{N} \frac{f_{jn}}{\alpha_j} \sum_{p=1}^{M} (\delta_{mp} - D_{jmp}) d_{jp}\right] = 0 \qquad (m = 1, M,\ n = 1, N). \end{aligned}\right\} \tag{32}$$

Here l_n, e_{jn} and f_{jn} are given in (A 2) and $DK\alpha_{jm}$, $DI\alpha_{jm}$, $DK\lambda_{nm}$ and $DI\lambda_{nm}$ are defined following (A 5). The coefficients A_{mp}, B_{nmp} and D_{jmp} are given in (28) where the summation $\sum''_{\alpha,\beta}$ is performed for a truncated prescribed value of $R_{\alpha\beta}$. The eigenvalues λ_n are obtained from (13), whereas the eigenvalues α_n and ν_n are evaluated numerically from (12) and (30) using Muller's method (Conte & Boor 1980).

Equation (32) constitutes $(3N+2)M$ equations, which can be solved for the $(3N+2)M$ unknowns: b_m, c_{nm} and d_{jm} $(m = 1, M,\ n = 0, N,\ j = 1, N)$. The d_{jm} are complex so each d_{jm} represents two unknowns, a real and an imaginary part. Once

(32) is solved by matrix algebra, all the unknowns except b_0 in (28) are known. b_0 is determined by applying the total flux condition in (6). This yields

$$b_0 = \frac{-3}{2(1+b_1 S \operatorname{Re}[g_1])}, \tag{33}$$

where $S = 2\pi/W^2$ and $g_1 = \mathrm{i}2\omega_1(\eta_2 - \eta_1)/\pi$.

3.4. *Drag coefficient*

From (1), the drag coefficient f is given by

$$f = \frac{\mu_{\text{eff}}}{\mu} = -\frac{B^2}{3}\left(\frac{\overline{\partial P}}{\partial x}\right). \tag{34}$$

Here the average pressure gradient $\overline{\partial P}/\partial x$ can be calculated from (7). Since the ϕ_n for $n > 0$ are doubly periodic functions, only the term involving ϕ_0 will contribute to the average pressure gradient. From the definition of $\overline{\partial P}/\partial x$,

$$f = -\frac{B^2}{3}\left(\frac{\overline{\partial P}}{\partial x}\right) = -\frac{B^2}{3}\frac{\langle P(Z+2\bar{\omega}_1+2\bar{\omega}_2)\rangle - \langle P(Z)\rangle}{W},$$

$$= -\tfrac{2}{3}(1 - b_1 S \operatorname{Re}[g_2])\, b_0 \tag{35}$$

where $\langle\ \rangle$ denotes an average over the z-direction and $g_2 = 2\omega_2(\eta_1+\eta_2)/\pi$. For a square array, $g_1 = g_2 = 1$ (Southard 1964). Substituting (33) into (35), we have

$$f = (1 - b_1 S)/(1 + b_1 S), \tag{36}$$

where it is seen that f depends only on the lowest-order coefficient b_1. The value of b_1, however, depends on the solution for all the coefficients in the truncated series.

4. Results

In this section, we shall first examine the convergence of the solutions and then present the results for the detailed velocity profiles, the drag coefficient, and the Darcy permeability as a function of aspect ratio B and fibre density S. The fluid velocity is calculated from (8)–(10) and the drag coefficient f is obtained from (36). A Brinkman approximation and an asymptotic formula are also given.

4.1. *Convergence of the solutions*

Extensive numerical tests have been conducted for the convergence of the solution as M, N, and N_{POST} (number of fibres in the quarter-plane) are increased. The criteria for convergence are: (*a*) the solution for the friction factor f converges to the desired number of digits, and (*b*) the no-slip conditions for $|v_r|$, $|v_\theta|$, and $|v_z|$ on the fibre surface do not exceed a prescribed error tolerance. The values of B_{nmp} and D_{nmp} in (28) are functions of B and S whereas A_{mp} is a function of S only. To test the effect of N_{POST} on the convergence of f, the values of f are calculated for $M = 2$ and $N = 1$. These values of N and M were chosen since the values of A_{mp}, B_{nmp}, and D_{nmp} in (28) converge faster as N_{POST} is increased for higher n, m, and p. Results not shown herein indicate that the solution for f converges much faster at the lower fibre density; e.g. for $B = 20$ and $S = 0.02$, one is able to assure five-digit convergence with $N_{\text{POST}} = 200$, while for $S = 0.2$, one can obtain only three-digit convergence with $N_{\text{POST}} = 2000$. The results also show that the value of N_{POST} required is a sensitive function of the aspect ratio B and that for $B \leqslant 5$, $N_{\text{POST}} \leqslant 200$ will be satisfactory for all $S \leqslant 0.2$.

The convergence tests as M and N are increased are shown in tables 1 and 2. Table

1 (*a*, *b*) presents the values of $|v_r|$, $|v_\theta|$, and $|v_z|$ on the fibre surfaces at $z = \frac{1}{2}B$ and $\theta = \frac{1}{4}\pi$ and thus the violation of the no-slip condition at this point. Table 2 shows the convergence for the friction factor f. These results are compared with Lee's (1969) two-term approximate solutions for $B = 1$, 5 and 20 and $S = 0.2$ and 0.02. Note $|v_z| = 0$ in Lee's two-term approximation since all the ϕ_n terms in (7)–(10) are neglected and there is neither a normal pressure gradient nor vertical velocity component. The interesting observation is that although Lee's solution provides reasonable agreement for f even when the aspect ratio is as large as 20 (error < 20% for $S < 0.2$), the no-slip conditions on the fibre surface are severely violated for $B \geqslant 5$. For instance, as shown in table 1 (*a*) for $S = 0.02$, the magnitude of v_r and v_θ on the fibre surface in Lee's approximate solution can exceed $0.37\bar{U}$ and $5.1\bar{U}$ for $B = 5$ and 20 respectively and the results for $S = 0.2$ are worse. The error in Lee's two-term approximation for the entire velocity profile will be shown in figures 2 and 3. Also shown in tables 1 and 2 are the effect of B and S on the rate of convergence. The results indicate that the n-series truncation N is mainly determined by the aspect ratio B. As observed in table 2, in order to obtain four-digit convergence for f at $S = 0.02$, N increases from 2, 4 to 10 for $B = 1$, 5 and 20 respectively. The m-series truncation M is only required at the larger value of $S = 0.2$. Four-digit convergence for $S = 0.02$ is achieved for f with $M = 1$. Additional results, not presented herein, indicate that for $B \leqslant 20$ solutions for f with at least four-digit accuracy can be achieved for $S \leqslant 0.5$ with $M = 4$.

4.2. *The velocity field*

The comparisons between the velocity profiles obtained by the present solution and the profiles predicted by Lee's (1969) two-term approximation are shown in figures 2 and 3. In figure 2 the velocity profiles along the radial coordinate at $z = \frac{1}{2}B$, $\theta = \frac{1}{4}\pi$ are plotted for $S = 0.02$ and $B = 5$. This figure shows clearly that Lee's approximation (the dotted curves) provides good results for v_r and v_θ for the far field but is a poor approximation for the boundary layer ($r/a < B$) surrounding the fibre surface.

The v_r, v_θ and v_z velocity profiles in the z-direction at four different radial positions, $r/a - 1 = 0, \frac{1}{8}\Delta, \frac{1}{4}\Delta, \frac{1}{2}\Delta$, along the $\theta = \frac{1}{4}\pi$ coordinate are plotted in figure 3. The values of S and B are the same as in figure 2. The solid lines in figure 3 represent the velocity profiles predicted by the present truncated series solution with $M = 2$, $N = 15$ and $N_{\mathrm{POST}} = 1000$. The velocity on the fibre surface is smaller than $0.0005\bar{U}$ everywhere and, therefore, would not be visible using the velocity scale in this figure. The results show that the velocity profiles for v_r and v_θ in the z-direction are nearly parabolic. The profile for v_z is determined by a linear combination of $Y_n(z)$ functions in (29). These functions require that v_z satisfy both the no-slip condition, $v_z(\pm B) = 0$, and the zero-gradient condition, $\partial v_z(\pm B)/\partial z = 0$. Since v_r and v_θ vanish on the channel walls, one can show from the continuity equation that $\partial v_z(\pm B)/\partial z = 0$. The dashed curves are the v_r and v_θ profiles obtained from Lee's (1969) two-term solution. The v_z velocity component is zero in Lee's approximation. The results indicate a maximum error at $z \approx 0.74B$. The two-term approximation introduced in Lee & Fung (1969) and used in Lee (1969) assumes that $1 - z^2/B^2 \approx 32\cos(\pi z/2B)/\pi^3$ in satisfying the no-slip conditions on the fibre surface. As noted in Lee & Fung (1969), this is a reasonable approximation only for $B < 1$. For larger values of B the no-slip condition is severely violated locally; however, as the results for the dashed curves labelled 1 indicate, the average value of v_r and v_θ is very roughly satisfied at the fibre surface. Since f is a global property, this explains why Lee's two-term approximation

N	$\lvert v_r\rvert$ $M=1$	$\lvert v_r\rvert$ $M=2$	$\lvert v_r\rvert$ $M=3$	$\lvert v_\theta\rvert$ $M=1$	$\lvert v_\theta\rvert$ $M=2$	$\lvert v_\theta\rvert$ $M=3$	$\lvert v_z\rvert$ $M=1$	$\lvert v_z\rvert$ $M=2$	$\lvert v_z\rvert$ $M=3$
				(a) $S=0.02$ and $N_{POST}=1000$					
Aspect ratio $B/a=20$									
Lee (1969)	5.6	5.1	5.1	5.8	6.4	6.3	0	0	0
2	2.8×10^{-2}	2.2×10^{-2}	2.2×10^{-2}	1.7×10^{-2}	1.2×10^{-2}	1.2×10^{-2}	0.12	0.12	0.11
4	6.4×10^{-2}	5.7×10^{-2}	5.7×10^{-2}	3.8×10^{-2}	4.4×10^{-2}	4.4×10^{-2}	9.5×10^{-2}	9.1×10^{-2}	9.1×10^{-2}
10	1.6×10^{-2}	1.5×10^{-2}	1.5×10^{-2}	7.8×10^{-3}	8.7×10^{-3}	8.7×10^{-3}	2.5×10^{-2}	2.4×10^{-2}	2.4×10^{-2}
15	4.9×10^{-3}	4.6×10^{-3}		3.3×10^{-3}	3.6×10^{-3}		1.8×10^{-3}	1.7×10^{-3}	
20	1.2×10^{-3}			3.7×10^{-4}			1.4×10^{-3}		
Aspect ratio $B/a=5$									
Lee	0.4	0.37	0.37	0.46	0.48	0.48	0	0	0
2	9.2×10^{-3}	8.6×10^{-3}	8.6×10^{-3}	5.4×10^{-3}	5.0×10^{-3}	5.0×10^{-3}	2.7×10^{-2}	2.6×10^{-2}	2.6×10^{-2}
4	5.1×10^{-3}	4.8×10^{-3}	4.8×10^{-3}	1.6×10^{-4}	4.7×10^{-5}	4.6×10^{-5}	1.3×10^{-2}	1.3×10^{-2}	1.3×10^{-2}
10	6.3×10^{-4}	5.9×10^{-4}	5.9×10^{-4}	2.0×10^{-4}	2.1×10^{-4}	2.1×10^{-4}	1.1×10^{-3}	1.0×10^{-3}	1.0×10^{-3}
15	1.5×10^{-4}	1.3×10^{-4}		2.9×10^{-4}	2.9×10^{-4}		7.8×10^{-5}	7.3×10^{-5}	
20	2.7×10^{-5}			1.1×10^{-5}			3.0×10^{-5}		
Aspect ratio $B/a=1$									
Lee	3.7×10^{-2}	3.7×10^{-2}	3.7×10^{-2}	8.2×10^{-2}	8.3×10^{-2}	8.3×10^{-2}	0	0	0
2	1.5×10^{-3}	1.5×10^{-3}	1.5×10^{-3}	3.3×10^{-3}	3.3×10^{-3}	3.3×10^{-3}	4.5×10^{-3}	4.5×10^{-3}	4.5×10^{-3}
4	4.7×10^{-4}	4.7×10^{-4}	4.7×10^{-4}	5.8×10^{-4}	5.8×10^{-4}	5.8×10^{-4}	1.5×10^{-3}	1.5×10^{-3}	1.5×10^{-3}
10	1.2×10^{-5}	1.2×10^{-5}	1.2×10^{-5}	3.3×10^{-5}	3.3×10^{-5}	3.3×10^{-5}	5.3×10^{-6}	5.1×10^{-6}	5.1×10^{-6}
15	4.7×10^{-6}	4.7×10^{-6}		8.1×10^{-5}	8.1×10^{-5}		1.7×10^{-6}	1.7×10^{-6}	
20	2.9×10^{-6}			2.5×10^{-6}			4.4×10^{-6}		

(*b*) $S = 0.2$ and $N_{\text{POST}} = 4000$

Aspect ratio $B/a = 20$									
Lee	22.0	4.4	4.3	33.0	55.0	55.0	0	0	0
2	0.80	0.22	0.22	1.3	2.1	2.1	3.7×10^{-2}	1.1×10^{-2}	1.2×10^{-2}
4	44×10^{-2}	0.12	0.10	0.16	0.12	0.10	8.9×10^{-2}	6.2×10^{-3}	1.0×10^{-2}
6	93×10^{-2}	0.49	0.22	1.1×10^{-2}	0.61	0.93	0.18	0.24	0.13
10	0.12	9.3×10^{-2}	9.0×10^{-2}	6.1×10^{-2}	9.2×10^{-2}	9.0×10^{-2}	0.20	0.18	0.17
15	47×10^{-2}	2.1×10^{-2}		3.6×10^{-2}	6.2×10^{-2}		1.5×10^{-2}	8.6×10^{-3}	
Aspect ratio $B/a = 5$									
Lee	1.4	0.30	0.29	2.1	3.5	3.5	0	0	0
2	1.7×10^{-4}	4.6×10^{-3}	6.6×10^{-3}	6.2×10^{-2}	7.0×10^{-2}	7.3×10^{-2}	6.2×10^{-2}	3.1×10^{-2}	3.0×10^{-2}
4	2.4×10^{-2}	8.3×10^{-3}	7.7×10^{-3}	3.6×10^{-3}	6.1×10^{-3}	5.5×10^{-3}	6.0×10^{-2}	3.1×10^{-2}	3.0×10^{-2}
6	4.0×10^{-2}	1.2×10^{-2}	1.1×10^{-2}	6.0×10^{-3}	2.3×10^{-2}	2.3×10^{-2}	9.3×10^{-2}	3.9×10^{-2}	3.9×10^{-2}
10	4.4×10^{-3}	1.4×10^{-3}	1.5×10^{-3}	1.3×10^{-3}	2.7×10^{-3}	2.8×10^{-3}	8.2×10^{-3}	2.9×10^{-3}	3.0×10^{-3}
15	1.3×10^{-3}	2.4×10^{-4}		1.7×10^{-3}	2.5×10^{-3}		6.5×10^{-4}	1.7×10^{-4}	
Aspect ratio $B/a = 1$									
Lee	6.8×10^{-2}	3.1×10^{-2}	3.2×10^{-2}	0.16	0.21	0.21	0	0	0
2	2.7×10^{-3}	1.4×10^{-3}	1.4×10^{-3}	6.2×10^{-3}	7.0×10^{-3}	7.0×10^{-3}	8.2×10^{-3}	4.4×10^{-3}	4.4×10^{-3}
4	8.9×10^{-4}	3.5×10^{-4}	3.6×10^{-4}	1.1×10^{-3}	1.2×10^{-3}	1.2×10^{-3}	2.8×10^{-3}	1.2×10^{-3}	1.2×10^{-3}
6	1.2×10^{-3}	3.1×10^{-4}	3.4×10^{-4}	2.8×10^{-4}	2.1×10^{-4}	2.0×10^{-4}	3.1×10^{-3}	9.1×10^{-4}	9.8×10^{-4}
10	2.7×10^{-5}	4.4×10^{-6}	2.9×10^{-7}	6.2×10^{-5}	7.8×10^{-5}	7.8×10^{-5}	1.8×10^{-5}	2.7×10^{-5}	2.4×10^{-5}
15	7.4×10^{-6}	9.5×10^{-6}		1.5×10^{-6}	1.9×10^{-4}		2.5×10^{-6}	4.5×10^{-6}	

TABLE 1. Convergence tests for no-slip condition for v_r, v_θ, and v_z on the fibre surface at $z = \frac{1}{2}B$ and $\theta = \frac{1}{4}\pi$

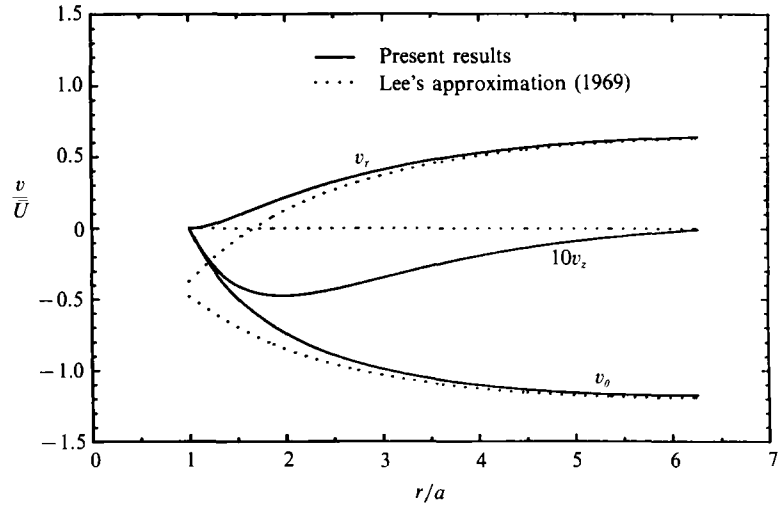

FIGURE 2. A comparison between the velocity profiles obtained by the present solution and the profiles predicted by Lee's (1969) two-term approximation. Profiles are shown in the $z = \frac{1}{2}B$ plane along a $\theta = \frac{1}{4}\pi$ coordinate for a fibre volume fraction $S = 0.02$ and an aspect ratio $B = 5$.

	$S = 0.02$			$S = 0.2$		
N	$M = 1$	$M = 2$	$M = 3$	$M = 1$	$M = 2$	$M = 3$
Aspect ratio $B = 20$						
Lee (1969)	11.632	11.634	11.634	507.56	533.62	533.61
2	10.876	10.878	10.878	442.81	465.27	465.26
4	10.871	10.872	10.872	433.45	454.96	454.95
6	10.869	10.871	10.871	429.45	448.59	448.47
10	10.897	10.898	10.898	436.28	458.31	458.31
15	10.893	10.895		432.83	454.56	
Aspect ratio $B = 5$						
Lee	1.7972	1.7973	1.7973	33.470	35.068	35.068
2	1.7759	1.7760	1.7760	30.671	32.041	32.041
4	1.7763	1.7764	1.7764	30.595	31.959	31.960
6	1.7763	1.7764	1.7764	30.550	31.908	31.908
10	1.7768	1.7768	1.7768	30.703	32.084	32.084
15	1.7768	1.7768		30.696	32.075	
Aspect ratio $B = 1$						
Lee	1.1113	1.1113	1.1113	3.0829	3.1235	3.1237
2	1.1102	1.1102	1.1102	3.0460	3.0843	3.0843
4	1.1103	1.1103	1.1103	3.0472	3.0855	3.0855
6	1.1103	1.1103	1.1103	3.0472	3.0856	3.0856
10	1.1103	1.1103	1.1103	3.0477	3.0861	3.0861
15	1.1103	1.1103		3.0477	3.0861	

TABLE 2. Convergence tests for friction factor f as N and M are increased. $N_{\text{POST}} = 1000$ for $S = 0.02$, $N_{\text{POST}} = 4000$ for $S = 0.2$

provides reasonable results for f for values of B for which the no-slip condition is very poorly satisfied pointwise. We shall take advantage of this property of orthogonal functions in developing an approximate formula for f later in the paper.

The change in the v_r, v_θ and v_z velocity profiles surrounding the fibres in the plane

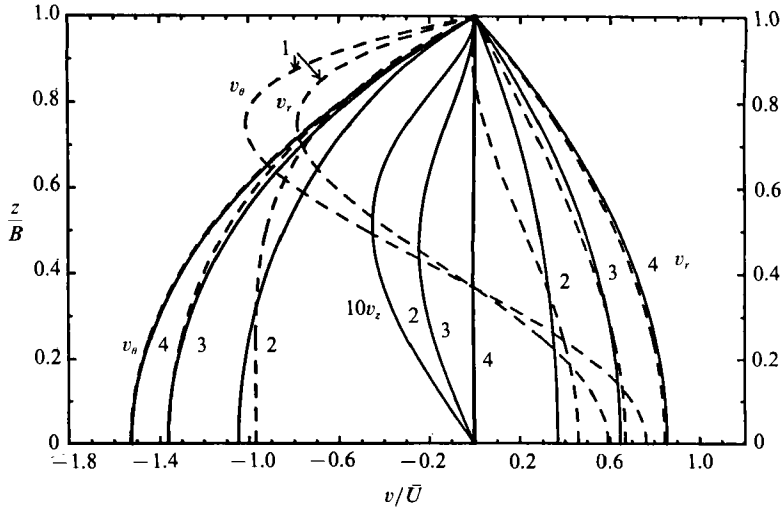

FIGURE 3. v_r, v_θ and v_z velocity profiles in the z-direction at four different radial positions, $(r-a)/a = O$ (curve 1), $\frac{1}{8}\Delta$ (2), $\frac{1}{4}\Delta$ (3) and $\frac{1}{2}\Delta$ (4) on line $\theta = \frac{1}{4}\pi$ joining fibre centres. Δ is the non-dimensional gap spacing between fibres. The dashed curves are the v_r and v_θ profiles obtained from Lee's (1969) two-term solution in which $v_z = 0$. The solid curves are predicted by the present solution. $S = 0.02$ and $B = 5$.

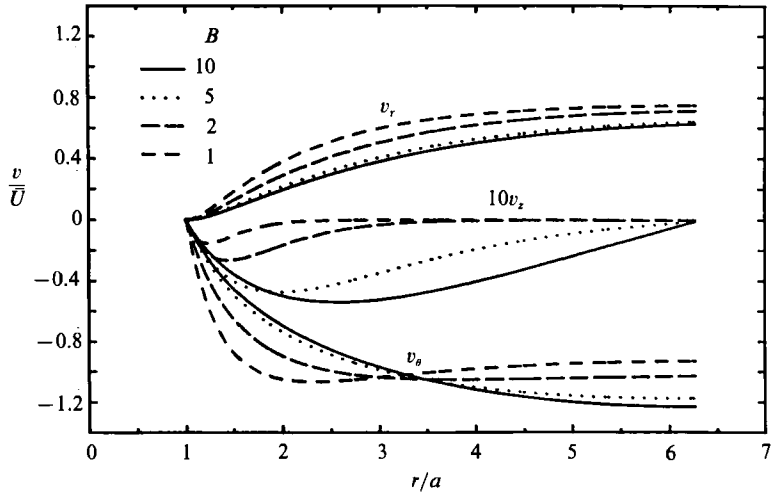

FIGURE 4. Solutions for v_r, v_θ, v_z velocity profiles along the $\theta = \frac{1}{4}\pi$ coordinate at $z = \frac{1}{2}B$ for fibres with varying aspect ratio B. The fibre volume fraction $S = 0.02$. Note that the magnitude of v_z is enlarged by a factor of 10.

$z = \frac{1}{2}B$ along $\theta = \frac{1}{4}\pi$ as B is increased, is shown in figure 4. Similar to the velocity profiles in Lee & Fung (1969) for a single fibre, the results reveal that v_z is significant only within a distance of the order of B from the fibre surface and its amplitude is one order of magnitude smaller than v_r and v_θ. The region where v_z is significant coincides with the viscous layer where the v_r and v_θ velocity components adjust to the no-slip conditions at the fibre surface. Outside this layer, the vertical velocity component is negligible and the fluid behaves like a two-dimensional Hele-Shaw flow. Later in this paper we shall show that the dimensionless thickness of this viscous layer δ, which is of $O(B)$, compared to the width of the open gap Δ between adjacent fibres is the critical condition for determining when the drag force due to the fibres

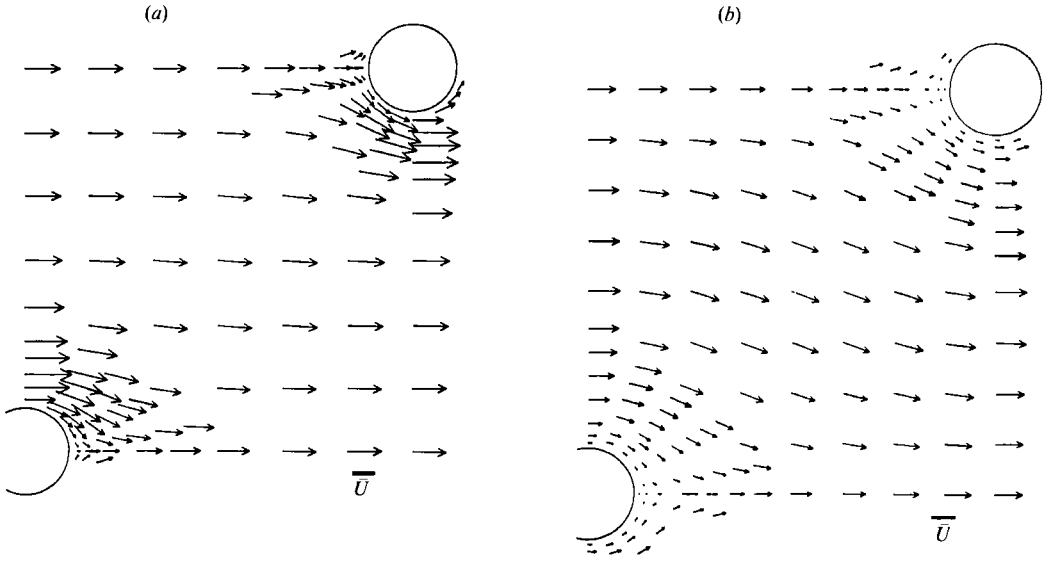

FIGURE 5. The velocity fields showing the viscous layers around the fibres at the centreplane ($z = 0$) for $S = 0.02$ and (*a*) aspect ratio $B = 0.5$ and (*b*) $B = 10$. The bar represents the magnitude of the average velocity $\bar{U}$.

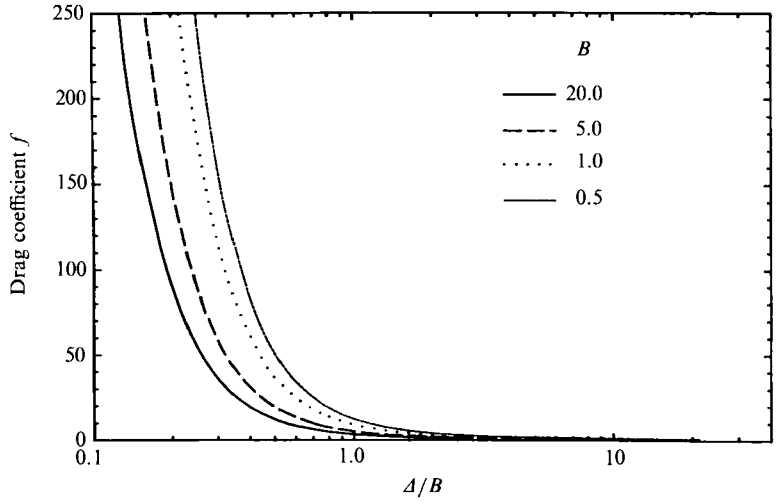

FIGURE 6. The drag coefficient f *vs.* the ratio of gap spacing to channel half-height Δ/B for four different aspect ratios B.

will cause the channel resistance to sharply increase. Figure 4 also shows that the magnitude of v_z decreases as the aspect ratio B decreases. This suggests that when S is fixed, Lee's (1969) two-term approximation will be approached provided B is small enough. Furthermore, in the limit $S \to 0$, i.e. $\Delta \gg 2B$, the flow will approach the solution in Lee & Fung (1969) for a single fibre. Similar to the behaviour exhibited by the v_z profiles in figure 3, where $\partial v_z/\partial z = 0$ on the two channel walls, one can show that v_r not only satisfies $v_r = 0$, but $\partial v_r/\partial r$ must also vanish on the fibre surfaces. The profiles in figure 4 exhibit this behaviour as $r/a \to 1$.

In figure 5(*a*, *b*), the velocity fields for $B = 0.5$ and 10 with the length of the velocity vector scaled to reflect $|\boldsymbol{v}|$ are plotted. The results are presented for the

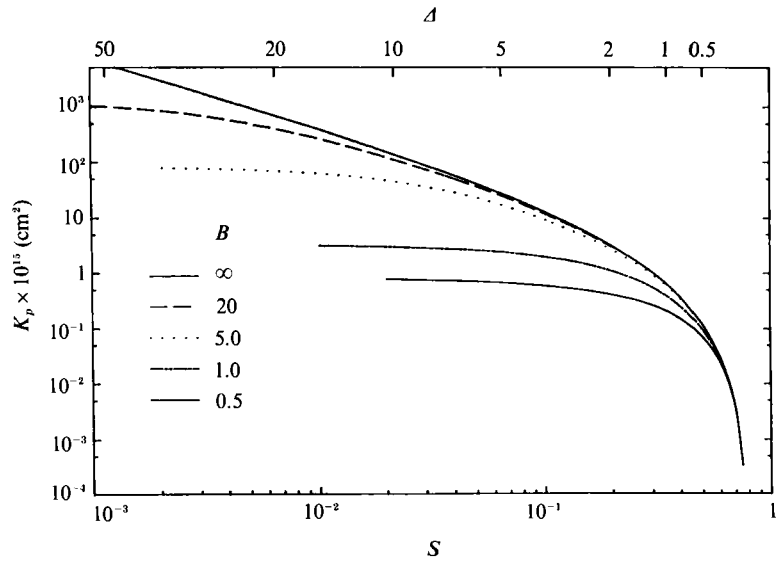

FIGURE 7. The Darcy permeability K_p plotted as a function of the fibre volume fraction S (bottom) and the dimensionless gap spacing Δ (top) for fibres of various aspect ratio B.

channel flow with $S = 0.02$ ($\Delta = 10.53$) at the centreplane ($z = 0$). One can clearly see the viscous layers surrounding the fibre surfaces. The viscous layers for $B = 0.5$ do not overlap and their thickness is much smaller than that for $B = 10$ at the same value of S.

4.3. *The drag coefficient f and Darcy permeability K_p*

A clearer insight into the mechanism which causes f to increase as B and S are increased is shown in figure 6. In this figure the drag coefficient f is plotted as a function of the ratio of the dimensionless gap spacing Δ to the dimensionless channel half-height B for four different aspect ratios, i.e. $B = 0.5$, 1, 5 and 20. This figure reveals that regardless of the value of B, the value of f starts to increase dramatically when the open gap between adjacent fibres becomes smaller than the scale of B. As shown in figure 4, the thickness of the viscous layer around the fibre surface is of order B. This strongly suggests that the sudden increase of f when $\Delta/B < O(1)$ is caused by the overlapping of the viscous layers.

The definition of the effective viscosity μ_{eff} given in (1) is based on a channel flow. This definition for μ_{eff} is not useful in describing the resistance of an infinitely long two-dimensional fibre array. In order to compare the transport properties obtained from two- and three-dimensional theories, we apply the definition for the Darcy permeability K_p as follows:

$$K_p = -\mu\bar{U}/\overline{\nabla' P'}. \tag{37}$$

For a channel flow, $K_p = B'^2/3f$, whereas for two-dimensional flow through a fibre array of infinite length, $K_p = W'^2/2f'_{2D}$ where $f'_{2D} = F/\mu\bar{U}$ and F is the drag force exerted by the fluid on a single fibre per unit fibre length. Therefore, an equivalent drag coefficient f_{2D} for a two-dimensional flow is defined as the following:

$$f_{2D} = \frac{2}{3}\left(\frac{B'}{W'}\right)^2 f'_{2D}. \tag{38}$$

Here f_{2D} is a function of S and B while f'_{2D} is a function of S only.

In figure 7, the Darcy permeability K_p is plotted against solid fraction S (bottom) and open gap Δ (top) for fibres of increasing aspect ratio B. The upper solid line

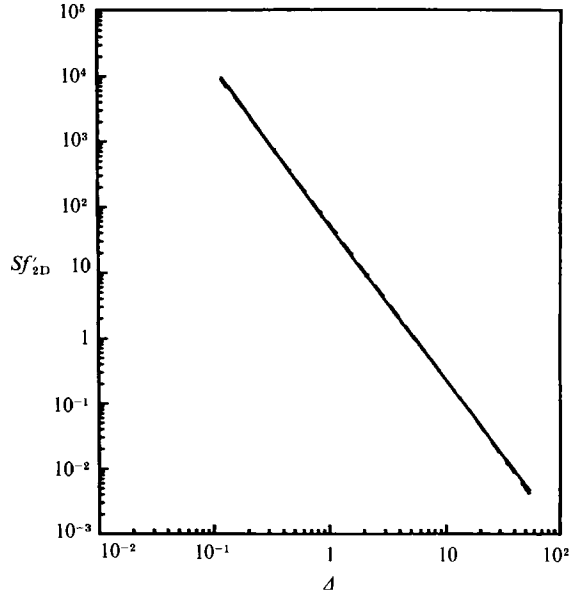

FIGURE 8. The results of curve fitting using equation (41) for the two-dimensional drag coefficient f'_{2D} (dashed curve). The solid curve represents the rigorous solution obtained by Sangani & Acrivos (1982).

($B = \infty$) is taken from Sangani & Acrivos (1982) for the two-dimensional limiting case. The results show that all the curves for different B merge with the two-dimensional limiting case if S is sufficiently high. This is because Δ decreases as S increases and B/Δ must eventually become $\gg 1$. In this limit, the viscous effects coming from channel wall are negligible compared to the viscous interaction between the fibres. In general, the larger the value of B the smaller the value of S at which K_p approaches the two-dimensional result.

4.4. *The Brinkman approximation*

The periodic fibre array in figure 1 can also be viewed as a porous medium bounded by two parallel channel walls. The effect of the channel walls on the Darcy flow can be approximately taken into account using a Brinkman equation (Bird *et al.* 1960; Ethier & Kamm 1989)

$$\nabla P = -\frac{\mu}{K_p} V + \mu \nabla^2 V, \tag{39}$$

which satisfies no-slip conditions at the top and bottom boundaries:

$$V = 0, \quad Z = \pm B. \tag{40}$$

If K_p, the Darcy permeability coefficient, is defined by its value for an infinite medium, (39) will reduce to Darcy's law in the dense fibre limit when K_p is small and to the standard Stokes equation in the opposite limit when K_p is large. In the present case K_p is given by $K_p = \pi a^2 / S f'_{2D}$ where f'_{2D} is obtained from the infinite two-dimensional solution in Sangani & Acrivos (1982). This solution for f'_{2D} is a complicated function of S. However, as shown in the log–log plot in figure 8, Sf'_{2D} is nearly a linear function of Δ and thus f'_{2D} is closely approximated by

$$f'_{2D} \approx \frac{54.95}{S\Delta^{2.377}}. \tag{41}$$

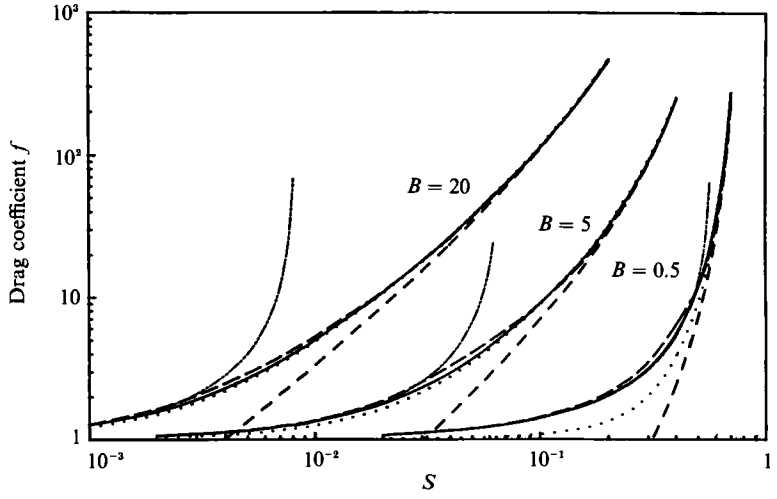

FIGURE 9. A comparison between the drag coefficients obtained by the present solution (——), the interpolation approximation (– – –) and the Brinkman approximation eq. (45) (· · · · ·). The two-term asymptotic solution of Lee (1969) (– · –), and the two-dimensional solution of Sangani & Acrivos (1982) (– – –), are also shown in the figure.

This formula is accurate to within 10% for $0.001 \leqslant S < 0.7$. Using (41), we obtain the following approximation for K_p:

$$K_p = 0.0572a^2\Delta^{2.377}. \tag{42}$$

If (39) is cast in dimensionless form, one can readily show that the magnitude of the viscous-layer thickness adjacent to the channel walls is of the order $K_p^{\frac{1}{2}}$. Therefore, for high fibre density, i.e. $K_p^{\frac{1}{2}}/B' \ll O(1)$, the channel wall effect is small and the results of the Brinkman equation approach the two-dimensional limiting solution except for the thin viscous layers in which the flow adjusts to satisfy the no-slip condition (40). On the other hand, when S is small, i.e. $K_p^{\frac{1}{2}}/B' \gg O(1)$, the porous material has little influence on the flow and the Brinkman equation will correctly predict the pure Poiseuille flow behaviour. Using the approximate expression for K_p in (42) one finds that $K_p^{\frac{1}{2}}/B' \sim \Delta^{1.1885}/B$. This relation confirms the results figure 6, which show that there is a transition from Hele-Shaw potential flow behaviour to viscous behaviour as Δ/B passes through unity. It is in the intermediate regime where $K_p^{\frac{1}{2}}/B'$ or Δ/B is of $O(1)$ that the Brinkman equation is of questionable validity.

The solution to (39) and (40) for the velocity profile in the channel is

$$V = -\frac{K_p}{\mu}\frac{\mathrm{d}P}{\mathrm{d}x}\left(1 - \frac{\cosh\left(z/K_p^{\frac{1}{2}}\right)}{\cosh\left(B'/K_p^{\frac{1}{2}}\right)}\right). \tag{43}$$

By averaging the velocity across the channel height, we can obtain an expression for the effective permeability,

$$K_{p,\mathrm{eff}} = -\mu\frac{V_{\mathrm{av}}}{\mathrm{d}P/\mathrm{d}x} = K_p\left(1 - \frac{\tanh\left(B'/K_p^{\frac{1}{2}}\right)}{B'/K_p^{\frac{1}{2}}}\right). \tag{44}$$

The drag coefficient f_{B} derived from this Brinkman equation is given by

$$f_{\mathrm{B}} = \frac{\eta^3}{3(\eta - \tanh\eta)} \tag{45}$$

where $\eta = (3f_{2\mathrm{D}})^{\frac{1}{2}} = B'/K_p^{\frac{1}{2}}$.

The solutions for f_B obtained from (45) are shown by the dotted curves in figure 9. These results indicate that the Brinkman approximation does approach the two-dimensional limit when $\Delta/B \ll 1$ and that curves with larger values of B will deviate from the two-dimensional solution at larger values of Δ, or smaller values of S. The results in figure 9 show that when B is larger than 5, the Brinkman approximation is a remarkably good approximation for all values of S, whereas when $B \leqslant O(1)$ the approximation deteriorates rapidly for S in the intermediate range. At these values of B the microstructure between the fibres can no longer be adequately represented by a Brinkman-type continuum equation. However, as will be shown next, a highly accurate interpolation formula can be developed for this range of B where the Brinkman approach breaks down.

4.5. *An asymptotic interpolation formula for f*

The results in figure 9 indicate that f derived from Lee's (1969) two-term asymptotic solution and the two-dimensional solution provide good approximations for both $\Delta/B \gg 1$ and $\Delta/B \ll 1$ respectively. This allows us to develop an accurate interpolation formula for the effective viscosity using a curve fit which asymptotically approaches the limiting expressions of Lee and Sangani & Acrivos. In Lee's two-term asymptotic solution the constant b_1 in (36) is given by

$$b_1 = \frac{K_2(\pi/2B)}{K_0(\pi/2B)}, \tag{46}$$

where K_n are modified Bessel functions of order n. The two-dimensional asymptotic expression is given by (38), where f'_{2D} is approximated by (41). These two asymptotic solutions provide the basis for developing a convenient interpolation formula for f which is valid for all values of S and B. Because there is no intersection between these two asymptotic solutions, the common interpolation formula

$$f = (f_{2D}^n + f_{3D}^n)^{1/n} \tag{47}$$

cannot be applied directly. Here f_{3D} represents Lee's asymptotic solution for $\Delta/B \gg 1$ and n is a free parameter that will be determined shortly. Since the solution given by (36) and (46) for f_{3D} breaks down rapidly when $\Delta < 2B$, f_{3D} is approximated by the tangent line at $S = S_\Delta$ for $S > S_\Delta$, where S_Δ is the solidity ratio when $\Delta = 2B$. This modified expression for f_{3D} for $S > S_\Delta$ is given by

$$f_{3D} = \left(\frac{1-b_1 S_\Delta}{1+b_1 S_\Delta}\right) - 2b_1 \frac{(S-S_\Delta)}{(1+b_1 S_\Delta)^2}. \tag{48}$$

Substituting (38) and (36) or (48) into (47) and requiring that the value of f at the intersection point of f_{2D} and f_{3D} match the numerical solution exactly, we can obtain a formula for n for different aspect ratios B:

$$n = B/(0.1918 + 0.3308B). \tag{49}$$

Some results of this interpolation approximation are plotted in figure 9. The formula is accurate to within 20% for all values of S when $B > 0.5$.

5. Concluding comments

As mentioned in the introduction, the motivation for this research derives from the study of the transcapillary exchange of water and hydrophilic solutes, where it has been hypothesized that cross-bridging proteoglycan fibres might exist throughout

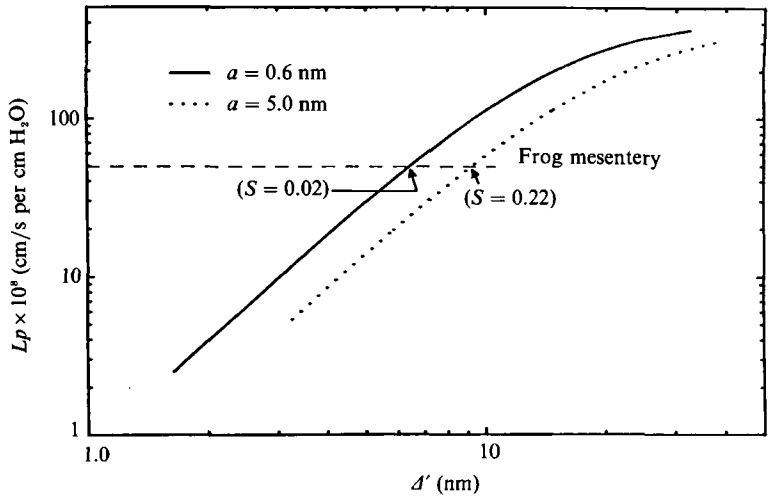

FIGURE 10. Solutions for the hydraulic conductivity Lp for a channel filled with a square array of cross-bridging fibres and with no junction strand. The horizontal dashed line indicates the value of Lp for frog mesentery capillary measured by Clough & Michel (1988). $2B' = 22$ nm, $L = 400$ nm.

the interendothelial clefts, Curry & Michel (1980). A new three-dimensional model has been proposed for capillary filtration through the clefts (channels) between the endothelial cells by Tsay *et al.* (1989). In this model the cleft consists of a channel with a junctional bar with periodically spaced missing proteins (pores) that separate two nearly uniform gap regions on the lumen and tissue fronts where the hypothesized cross-bridging fibre matrix is present. The results of this study can be applied to the model for the hydraulic resistance of the fibre matrix in the wide portions of the cleft on each side of the junction bar. Physiologists measure this resistance in terms of an hydraulic conductivity per cm^2 of endothelial surface L_p. The hydraulic conductivity for a cleft without a junctional bar is related to K_p by $L_p = K_p(2B'L_{jt}/\mu L)$, where L_{jt} is the total junction length per unit capillary surface area and L is the depth of the cleft. The cleft dimensions used in figure 10, $L = 400$ nm, $B' = 11$ nm and $L_{jt} = 2000$ cm/cm^2, are based on the values for frog mesentery capillary measured by Clough & Michel (1988). The solid curve is for a cleft with slender cross-bridging proteoglycan fibres of 0.6 nm radius, the dotted curve is for cross-bridging proteins of 5 nm radius, and the dashed horizontal line shows the values of L_p for frog mesentery capillary measured by Clough & Michel (1988).

The results in figure 10 indicate that the measured value of L_p for frog mesentery can be achieved by a cleft with no junctional bar and fibres of 0.6 nm radius occupying approximately 2% of the cleft volume. The open gap Δ' between adjacent fibres for this fibre density is 6.3 nm. Thus, for a cleft with most of its tight junction open (little or no junctional bar), the fibre matrix could possibly serve as the primary molecular sieve for the intermediate size solutes of less than 6 nm diameter. The present results, however, represent the smallest fibre spacing possible since they neglect the resistance of the junction bar entirely. It is suggested in Tsay *et al.* (1989) that the junction pores, if formed by missing junction proteins, would have just the right dimensions (approximately 5–6 nm radius) for the junction strand with its pores to serve as the molecular sieve. Widely spaced small gaps of this nature have been observed by Bundgaard (1984) in serial section electron microscopic reconstructions of the junction strands. The presence of a junction strand with this

ultrastructure greatly increases the hydraulic resistance of the cleft and would significantly increase the minimum fibre spacing required for a combined model of junction pores and fibres to correctly predict the measured value of L_p. Further experiments are therefore required to determine whether the pores in the junction bar or the fibre matrix serves as the principal molecular filter. It has also been suggested that bridging proteins of 5 nm radius might provide the uniformity of gap height that is observed in the wide portion of the cleft of all endothelial cells. The dotted curve in figure 10 is the prediction for this hypothetical model. These molecules would have to have a minimum Δ' of 9 nm, or centre-to-centre spacing of 19 nm ($S = 0.22$), to account for the measured value of L_p. While this protein spacing is highly unlikely, one could have widely spaced bridging proteins that have no significant effect on L_p. A biological paper describing the complete model for the flow in the interendothelial cleft has been submitted elsewhere (Weinbaum, Tsay & Curry 1991).

In summary, we have developed in this study a highly accurate doubly infinite series solution for flow through a square array of cylindrical fibres confined between two parallel walls. The solution successfully describes the interaction for the fibre array wherein the flow ranges from the irrotational Hele-Shaw limit ($B \ll 1$) to the viscous two-dimensional limiting case ($B \gg 1$). A viscous layer with scale of order B is found on the fibre surface. The vertical velocity component is only significant within this viscous layer. When the viscous layers surrounding the fibres overlap, the drag coefficient of the fibrous bed increases dramatically. Our results show that instead of S and B, Δ/B is the best parameter to judge whether the fibre array can be described by a two-dimensional approximation. When $\Delta/B \gg 1$, the fluid streamlines exhibit a potential flow behaviour, except in a thin region of $O(B)$ around the fibre surfaces. In contrast to classic Hele-Shaw flow it is not necessary for $B \ll 1$ for this potential outer flow to exist. Finally, the present study shows that the Brinkman equation provides a very good approximation when $B > 5$ but deteriorates rapidly for $B < O(1)$. An alternative asymptotic interpolation formula which is accurate to within 20% for all values of S and $B > 0.5$ is also developed.

The authors gratefully acknowledge the support of NSF grant CTS-8803116 and NIH grant HL-19454. This research was performed in partial fulfilment of the requirements for the Ph.D. degree of R. Tsay from the City University of New York.

Appendix

Orthogonal expansions for the various functions of z appearing in (7)–(10) can be written in the form

$$1-\left(\frac{z^2}{B^2}\right) = \sum_{n=0}^{\infty} l_n \cos\lambda_n z, \quad -\frac{1}{\alpha_j}\frac{\mathrm{d}q_j}{\mathrm{d}z} = \sum_{n=0}^{\infty} e_{jn}\cos\lambda_n z, \quad q_j(z) = \sum_{n=1}^{\infty} f_{jn}\, Y_n(z), \tag{A 1}$$

where λ_n is given by (13) and

$$l_n = \frac{32(-1)^n}{\pi^3(2n+1)^3}, \quad e_{jn} = \frac{4(-1)^n\lambda_n\alpha_j}{B^2(\alpha_j^2-\lambda_n^2)^2}, \tag{A 2}$$

$$f_{jn} = \frac{8\sqrt{2}\nu_n^3\alpha_j^3}{B^2(\nu_n^4-\alpha_j^4)^2}\left[\tan\alpha_j B\coth\nu_n B - \frac{\alpha_j}{\nu_n}\right].$$

The expressions for $\bar{U}_{mn}$, $\bar{V}_{mn}$ and $\bar{W}_{mn}$ appearing in (31) are given by the following:

$$\bar{U}_{mn}(r) = l_n\left(\delta_{m1} + b_m r^{-2m} + \sum_{p=1}^{\infty} A_{mp} b_p r^{2m-2}\right) + \frac{(2m-1)}{\lambda_n r}\left[c_{nm} K\lambda_{nm} + \sum_{p=1}^{\infty} B_{nmp} c_{np} I\lambda_{nm}\right] + \mathrm{Re}\sum_{j=1}^{\infty}\left[\frac{e_{jn}}{\alpha_j^2}\left(-d_{jm} DK\alpha_{jm} + \sum_{p=1}^{\infty} D_{jmp} d_{jp} DI\alpha_{jm}\right)\right], \tag{A 3}$$

$$\bar{V}_{mn}(r) = l_n\left(\delta_{m1} - b_m r^{-2m} + \sum_{p=1}^{\infty} A_{mp} b_p r^{2m-2}\right) + \frac{1}{\lambda_n}\left[c_{nm} DK\lambda_{nm} + \sum_{p=1}^{\infty} B_{nmp} c_{np} DI\lambda_{nm}\right] + \mathrm{Re}\sum_{j=1}^{\infty}\left[\frac{(2m-1)\, e_{jn}}{\alpha_j^2 r}\left(-d_{jm} K\alpha_{jm} + \sum_{p=1}^{\infty} D_{jmp} d_{jp} I\alpha_{jm}\right)\right], \tag{A 4}$$

$$\bar{W}_{mn}(r) = \mathrm{Re}\sum_{j=1}^{\infty}\frac{f_{jn}}{\alpha_j}\left(d_{jm} K\alpha_{jm} - \sum_{p=1}^{\infty} D_{jmp} d_{jp} I\alpha_{jm}\right), \tag{A 5}$$

where

$$K\alpha_{jm} = \frac{K_{2m-1}(\alpha_j r)}{K_{2m-1}(\alpha_j)}, \quad I\alpha_{jm} = \frac{I_{2m-1}(\alpha_j r)}{I_{2m-1}(\alpha_j)},$$

$$K\lambda_{nm} = \frac{K_{2m-1}(\lambda_n r)}{K_{2m-1}(\lambda_n)}, \quad I\lambda_{nm} = \frac{I_{2m-1}(\lambda_n r)}{I_{2m-1}(\lambda_n)},$$

$$DK\alpha_{jm} = \frac{K'_{2m-1}(\alpha_j)}{K_{2m-1}(\alpha_j)}, \quad DI\alpha_{jm} = \frac{I'_{2m-1}(\alpha_j)}{I_{2m-1}(\alpha_j)},$$

$$DK\lambda_{nm} = \frac{K'_{2m-1}(\lambda_n)}{K_{2m-1}(\lambda_n)}, \quad DI\lambda_{nm} = \frac{I'_{2m-1}(\lambda_n)}{I_{2m-1}(\lambda_n)},$$

$$K'_m = \frac{\mathrm{d}K_m}{\mathrm{d}r}, \qquad I'_m = \frac{\mathrm{d}I_m}{\mathrm{d}r}.$$

REFERENCES

Bird, R., Stewart, W. & Lightfoot, E. 1960 *Transport Phenomena*. Wiley.

Brinkman, H. C. 1947 *Physica* **13**, 447.

Bundgaard, M. 1984 *J. Ultrastruct. Res.* **88**, 1.

Clough, G. & Michel, C. C. 1988 *J. Physiol.* **405**, 563.

Conte, S. D. & Boor, C. D. 1980 *Elementary Numerical Analysis*. McGraw-Hill.

Curry, F. E. 1984 Transcapillary exchange. In *Handbook of Physiology* (ed. E. M. Renkin & C. C. Michel), sect, 2, The Cardiovascular System, Vol. 4, The Microcirculation, Bethesda, Md, American Physiological Society, 309.

Curry, F. E. 1986 *Circulat. Res.* **59**, 367.

Curry, F. E. & Michel, C. C. 1980 *Microvasc. Res.* **20**, 96.

Drummond, J. E. & Tahir, M. I. 1984 *Intl J. Multiphase Flow* **10**, 515.

Ethier, C. R. & Kamm, R. D. 1989 *PhysicoChem. Hydrodyn.* **11**, 219.

Firth, J. A., Bauman, K. F. & Sibley, C. P. 1983 *J. Ultrastruct. Res.* **85**, 45.

Fung, Y. C. & Sobin, S. S. 1969 *J. Appl. Physiol.* **26**, 472.

Happel, J. 1959 *AIChE J.* **5**, 174.

Hele-Shaw, H. S. 1898 *Nature* **58**, 34.

Kuwabara, S. 1959 *J. Phys. Soc. Japan* **14**, 527.

Larson, R. E. & Higdon, J. J. L. 1986 *J. Fluid Mech.* **166**, 449.

Lee, J. S. 1969 *J. Biomech.* **2**, 187.

LEE, J. S. & FUNG, Y. C. 1969 *J. Fluid Mech.* **37**, 657.

MICHEL, C. C. 1985 Malpighi Award Lecture. *Intl J. Microcirculat. Clin. Exp.* **4**, 265.

NEALE, G. & NADER, W. 1974 *Can. J. Chem. Engng* **52**, 475.

O'BRIEN, R. W. 1979 *J. Fluid Mech.* **91**, 17.

PERRINS, W. T., MCKENZIE, D. R. & MCPHEDRAN, R. C. 1979 *Proc. R. Soc. Lond.* A **369**, 207.

RAYLEIGH, LORD 1892 *Phil. Mag.* **34**, 481.

SANGANI, A. S. & ACRIVOS, A. 1982 *Intl J. Multiphase Flow* **8**, 193.

SILBERBERG, A. 1987 Passage of macromolecules and solvent through clefts between endothelial cells. In *Microcirculation – an Update* (ed. M. Tsuchiya *et al.*), vol. 1, p. 153. Elsevier.

SOUTHARD, T. H. 1964 Weierstrass elliptic and related functions. In *Handbook of Mathematical Functions* (ed. M. Abramowitz & I. A. Stegun), p. 627. Dover.

SPIELMAN, L. & GOREN, S. L. 1968 *Environ. Sci. Tech.* **2**, 279.

THOMPSON, B. W. 1968 *J. Fluid Mech.* **31**, 397.

TSAY, R., WEINBAUM, S. & PFEFFER, R. 1989 *Chem. Engng Commun.* **82**, 67.

WATSON, G. N. 1980 *A Treatise on the Theory of Bessel Functions.* Cambridge University Press.

WEINBAUM, S. 1980 *J. Theor. Biol.* **83**, 63.

WEINBAUM, S., GANATOS, P. & YAN, Z. Y. 1990 *Ann. Rev. Fluid Mech.* **22**, 275.

WEINBAUM, S., TSAY, R. & CURRY, F. E. 1991 A three dimensional model for permeability of endothelial clefts with junction strand and fiber matrix components. (Submitted.)

WHITTAKER, E. T. & WATSON, G. N. 1944 *A Course of Modern Analysis.* Cambridge University Press.